THE USE OF FRFT IN RADAR SYSTEMS FOR SPACE DEBRIS SURVEILLANCE

Yuan Zhen-tao, Hu Wei-dong, Yu Wen-xian

ATR State Key Lab. National University of Defense Technology Changsha, Hunan Province, China
Email: nudtvellon@163.com.cn

ABSTRACT

This paper discusses the application of fractional Fourier transform (FrFT) to deal with target detection and parameters estimation in radar systems for space debris surveillance. The analytical expressions of the velocity and acceleration are obtained with some simplifications performed at first. Then the radar echo model is built based on the analysis of the motion characteristics. The detection performance of fast Fourier transform (FFT) and FrFT are compared after the expression of the maximum integration time of FFT is derived. Finally, the parameters estimation accuracy of FrFT is analysed. The results indicate that FrFT could achieve considerable enhancement for debris detection with the efficient energy accumulation. It is also shown that the parameters estimation accuracy of FrFT is quite close to CRLB (Cramer-Rao Lower Bounds).

1. INTRODUCTION

Recently, space debris surveillance and cataloging have got more and more focus from many countries with the increasing space activities. As known to all, radar systems have superior performance for low earth orbit (LEO) space debris surveillance, such as "all-the-time and all-weather" functionality. Considering the large number and wide distribution of space debris, the preferred way for general survey is to form a large-scale electromagnetic fence, e.g. American "Navy Space Surveillance System" [1] and French "Graves" [2].

Besides increasing the power aperture product of radar hardware, another effective way for detecting small size space debris is to increase the coherent integration time. However, space debris velocities with respect to the radar will change when crossing the radar field-in-view (FOV) and result in the Doppler frequency shift. Such inconstant Doppler frequencies lead to a significant decrement in the energy accumulation efficiency of traditional coherent integration techniques, such as Fourier transform (FT). To deal with this problem, it's essential to exploit the potential of time-frequency analysis techniques for improving integration gain.

Short time FT (STFT) and wavelet Transform (WT) approaches are well-known time-frequency analysis techniques [3]. However, affected by the window function inevitably, their detection performance is degraded and time-frequency domain resolution is restricted. By means of integral over a line in the time-frequency plane, WVD-HT (Wigner-Ville Distribution & Hough-Transform) approach can concentrate the energy of a signal and get rid of the disturbance induced by the cross-terms. However, WVD-HT requires time-consuming computation and loses the phase [4, 5]. Fractional Fourier transform (FrFT) is a generalization of FT, which can be regarded as a counter clockwise rotation of the signal coordinates around the origin in the time-frequency plane. By obtaining the Doppler shift and the chirp rate of a signal simultaneously, FrFT can accumulate the reflected energy efficiently. Thus, the detection performance and the accuracy of parameters estimation could be highly improved. Moreover, FrFT has a remarkably computational efficiency for it can be computed by fast Fourier transform (FFT) [6]. Furthermore, the detection and parameter estimation for multi-component signal could be easily achieved via FrFT filtering and Inverse FrFT.

This paper discusses the application of FrFT in radar signal processing for space debris surveillance. The movement of space debris crossing the radar FOV is formulized at first, and then the analytical expressions of the velocity and acceleration are obtained with some simplifications performed. Based on the motion characteristics analysis, the radar echo model is built. After the analytic derivation of the maximum integration time of FFT was derived, the detection performance of FFT and FrFT are compared. Finally, the parameters estimation accuracy of FrFT is analyzed. The results indicate that FrFT could achieve considerable enhancement compared with FFT for LEO debris detection. Additionally, the parameters estimation accuracy of FrFT is quite close to their Cramer-Rao lower bounds (CRLB).

2. RADAR ECHO MODEL OF SPACE DEBRIS

2.1. Geometrical Relation between Space Debris and Survey Station

The geometry of space debris observation is depicted firstly. Fig. 1-a is the basic geometry of space debris observation. A segment of the space debris's orbit and the corresponding segment of the ground trace are shown in the figure. The coordinate system is an earth centred fixed (ECF) coordinate system. P denotes the location of the survey station. Let t_0 denotes the instant when the survey station observes maximum elevation

Proc. '5th European Conference on Space Debris', Darmstadt, Germany
30 March – 2 April 2009, (ESA SP-672, July 2009)

angle. S_0 is the location of the space debris at maximum elevation angle and E is the corresponding sub-satellite point. Consider the Fig. 1-b, $\theta(t)$ is the observation elevation angle, $\gamma(t)$ is the geocentric angle between survey station and the sub-satellite point and $d(t)$ is the distance between the survey station and the space debris. R_E is the radius of the earth. Fig. 1-c is the spherical triangle of DEP, and $\psi(t)$-$\psi(t_0)$ is the angular distance between D and E measured on the surface of earth along the ground trace.

By the law of cosines applied to the plane triangle shown in Fig. 1-b, the slant range $d(t)$ is determined.

$$d(t) = \sqrt{R_E^{\,2} + R^2 - 2R_E R \cdot \cos[\gamma(t)]} \tag{1}$$

By the cosine law of sides applied to the spherical triangle shown in Fig. 1-c, we obtain

$$\cos[\gamma(t)] = \cos[\psi(t) - \psi(t_0)] \cdot \cos[\gamma(t_0)] \tag{2}$$

The maximum elevation angle $\theta_{\max}$ also satisfies

$$\cos(\theta_{\max} + \gamma(t_0)) = \cos(\theta_{\max}) R_E / R \tag{3}$$

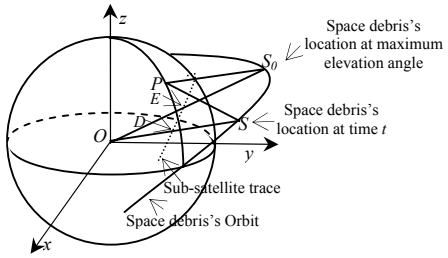

Figure 1-a. Geometry of space debris detection

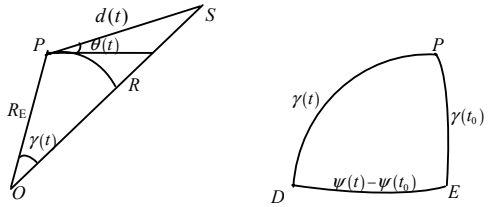

Figure 1-b. Plane triangle Figure 1-c. Spherical triangle

2.2. Analysis of Space Debris Motion Characteristics

Substituting Eq. 2 in Eq. 1 and differentiating the expression, we get the relative velocity of space debris with respect to the survey station

$$v(t) = \frac{R_E R \cdot \cos[\gamma(t_0)] \sin[\psi(t) - \psi(t_0)] \cdot \dot{\psi}(t)}{\sqrt{R_E^{\,2} + R^2 - 2R_E R \cdot \cos[\gamma(t_0)] \cos[\psi(t) - \psi(t_0)]}} \tag{4}$$

where $\dot{\psi}(t)$ is the angular velocity of the space debris in the ECF frame. As in [7], we have $\dot{\psi}(t) = \omega_F(t) \approx \omega_S - \omega_E \cos(I) = \omega_0$, where ω_S denotes the angular velocity of the space debris in the earth centred inertial (ECI) coordinate system, ω_E denotes the angular velocity of Earth's rotation and I denotes the inclination of space debris orbit. Differentiating Eq. 4, we obtain the acceleration of space debris

$$a(t) \approx \frac{R_E R \cdot \omega_0^{\,2} \cos[\gamma(t_0)] \cdot \cos[\Delta\psi]}{\sqrt{R_E^{\,2} + R^2 - 2R_E R \cdot \cos[\gamma(t_0)] \cos[\Delta\psi]}} - \frac{\omega_0^{\,2} \cdot (R_E R \cdot \cos[\gamma(t_0)] \cdot \sin[\Delta\psi])^2}{\left(\sqrt{R_E^{\,2} + R^2 - 2R_E R \cdot \cos[\gamma(t_0)] \cos[\Delta\psi]}\right)^3} \tag{5}$$

where $\Delta\psi = \omega_0 (t - t_0)$. Let t_v denotes the time when the space debris just become visible to the survey station. $\theta_{\min}$ is the minimum elevation angle observed at t_v. we can obtain

$$|t_v - t_0| \approx \frac{1}{\omega_0} \times \cos^{-1}\left(\frac{\cos\left(\cos^{-1}(R_E \cos\theta_{\min} / R) - \theta_{\min}\right)}{\cos\left(\cos^{-1}(R_E \cos\theta_{\max} / R) - \theta_{\max}\right)} \right) \tag{6}$$

$T_d = |t_v - t_0|$ denotes the total visibility duration of the debris at the survey station. For LEO space debris, the effect caused by orbit inclination I on ω_0 is negligible. According to Eq. 4 and Eq. 5, we provide numerical results for velocity and acceleration of space debris with respect to the survey station versus time with $\theta_{\max}$ ranging from $\pi/4$ to $\pi/2$. Time is expressed relative to the zero Doppler instant, at which the elevation angle from the survey station to the space debris is at its maximum value. Fig. 2 shows the velocity and acceleration of the space debris at the survey station for the visibility duration. The space debris follows a circular orbit of altitude 1000 Km.

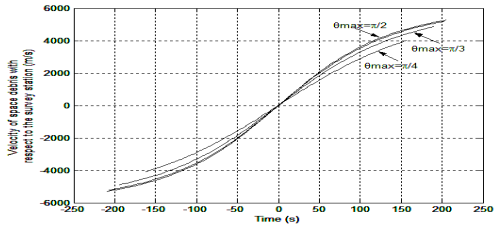

Figure 2-a. Velocity versus time for different $\theta_{\max}$

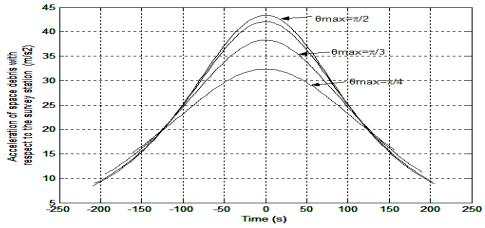

Figure 2-b. Acceleration versus time for different $\theta_{\max}$

The minimum elevation angle θ_{min} is assumed as $\pi/6$, which is rational for most space surveillance systems. As shown in Fig. 2, the visibility duration increases as the maximum elevation angle increases. The acceleration of space debris is time-variant and reaches its maximum value at the maximum elevation angle. As analysed, the acceleration of space debris with respect to the survey station $a(t)$ is relevant to θ_{min}, θ_{max} and the orbit altitude H, which is a function of elevation angle $\theta(t)$. The mean of $a(t)$ at different θ_{min} and H is presented in Fig. 3. The influence of θ_{max} on the mean of $a(t)$ is almost negligible according to the numerical results which are omitted here.

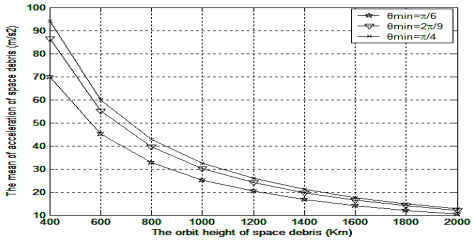

Figure 3. Mean of a(t) versus altitude at different θ_{min}

When survey station observes space debris, $\theta(t)$ changes from θ_{min} to θ_{max} and becomes θ_{min} at last. Due to the limited radar FOV, the observation is part of that process. $\theta(t)$ can be regarded as obeying uniform distribution between θ_{min} and θ_{max}, therefore using the mean of $a(t)$ to describe the acceleration is rational and meaningful.

2.3. Radar Echo Model of Space Debris

In radar observation, the amplitude, time delay and phase of echo signal are changing with time because of the movement of targets. The echo amplitude is considered as constant in a short period. Take "NAVSPASUR" for instance, the crossing time is at the level of 10^{-1}s [8]. Thereby the radar echo signal can be written as follows:

$$r(t) = b \cdot s\left(t - \tau(t)\right)\exp\left(-\mathrm{j}\omega_0\tau(t)\right) \tag{7}$$

where b is the echo amplitude, $s(t)$ denotes the emission signal, $\tau(t)$ is the time delay and j represents the imaginary unit. According to the analysis above and considering the short crossing time, the movement of space debris can be modelled as a constant acceleration motion. After the match filter, the radar echo is a LFM signal, which is given by [9]

$$r'(t) = b \cdot \exp\left(-\mathrm{j}(\varphi + 2\pi f_0 t + \pi\xi_0 t^2)\right) \quad |t| \le T/2 \tag{8}$$

where $f_0=2v_0/\lambda$ denotes the Doppler shift and $\xi_0=2a/\lambda$ denotes the chirp rate of the signal. λ denotes the wavelength of the emission signal, v_0 is the radial velocity at middle time and a is the acceleration of target with respect to the receiver. T denotes the observation duration. For the radar FOV with certain thickness, the movement can be modelled as a subsection constant acceleration motion. The model of each section also can be expressed in the form of Eq. 8.

3. DETECTION PERFORMANCE OF FRFT

3.1. Detection Performance of FFT for Constant Acceleration Motion

FFT is a common technique for moving target detection. This section discusses the detection performance of FFT from the point of view of cumulative gain in Signal Noise Ratio (SNR). The FT of echo signal is given by

$$B(\omega) = b \cdot \int_{-T/2}^{T/2} r'(t)\exp(-\mathrm{j}\omega t)dt \tag{9}$$

According to the model established above, Eq. 9 can be written as $B(\omega) = Tb \cdot Sinc\left[(\omega + 2\pi f_0)T/2\right]e^{-\mathrm{j}\varphi}$ if $\xi_0=0$ and $|B(\omega)|^2$ reaches its maximum value T^2b^2 at $\omega=-2\pi f_0$. If $\xi_0\neq 0$, Eq. 9 can be rewritten as

$$|B(\omega)| = \frac{b}{2\left|\sqrt{\xi_0}\right|} \cdot \left| \begin{pmatrix} \mathrm{Erfi}\left[C \cdot (-2f_e + \xi_0 T)/\sqrt{\xi_0}\right] \\ +\mathrm{Erfi}\left[C \cdot (2f_e + \xi_0 T)/\sqrt{\xi_0}\right] \end{pmatrix} \right| \tag{10}$$

where $C = (-1)^{3/4}\sqrt{\pi}/2$ and $f_e = f_0 + \omega/2\pi$. $\mathrm{Erfi}(z) = 2/\left(\mathrm{j}\sqrt{\pi}\right) \cdot \int_0^{\mathrm{j}z} \exp(-t^2)dt$, which is the imaginary error function. Usually, the signal is sampled. The FFT of Eq. 8 is given by

$$\begin{aligned} B(k) &= b \cdot \sum_{n=-N/2}^{N/2} r'(n)\exp\left(-\mathrm{j}2\pi kn/(N+1)\right) \\ &= F \cdot B(\omega) \cdot \delta\left(\omega - 2\pi Fk/(N+1)\right) \quad |k| \le N/2 \end{aligned} \tag{11}$$

where F is the sampling frequency and $N+1 = FT$. The noise $e(t)$ is assumed to be an additive white gauss noise (WGN). We define $SNR_{out}=J(k)/L(k)$ and $SNR_{in}=b^2/\sigma^2$ as the output and input SNR respectively, where $J(k)$ and $L(k)$ denotes the power spectrum of signal and noise.

Let SNR_{MF} denotes the optimal output SNR, and we have $SNR_{MF}=(N+1)\,b^2/\sigma^2$.The cumulative gain in SNR is defined by

$$\begin{aligned} G_{SNR}(\omega) &= SNR_{out}/SNR_{MF} = |B(\omega)|^2/T^2b^2 \\ \omega &= 2\pi F \cdot k/(N+1), |k| \le N/2 \end{aligned} \tag{12}$$

Substitution of $p = f_e \cdot T$ and $q = \sqrt{\xi_0} \cdot T$ into Eq. 10 yields the following expression:

$$G_{\text{SNR-FFT}}(\omega) = 1\Big/\left(4|q|^2\right) \cdot \left| \begin{pmatrix} \text{Erfi}\left[C \cdot \left(-2p + q^2\right)/q\right] \\ +\text{Erfi}\left[C \cdot \left(2p + q^2\right)/q\right] \end{pmatrix} \right|^2 \quad (13)$$

where $\omega = 2\pi F \cdot k/(N+1), |k| \le N/2$. If k_0=-f_0(N+1)/F, which can be achieved easily by FFT interpolation [10], then we have ω_0=-2πf_0. By the definition of f_e and p, we get p_{k0}=0. Let k_1=k_0+1, p_{k1}=1. By means of numerical computation, we obtain that $G_{\text{SNR-FFT}}(k_1)$ exceeds $G_{\text{SNR-FFT}}(k_0)$ for the first time when $|q|$=q_0 ≈ 2.17329. For $G_{\text{SNR-FFT}}$ being symmetrical around p, there are two distinguishable peaks, which means the false alarm appears. The detection performance of FFT degrades with the increase of $|q|$ because the value of the peak decreases. The FFT approach is invalid when $|q| \ge q_0$ for the false alarm caused by the split of $G_{\text{SNR-FFT}}$, as shown in Fig. 4.

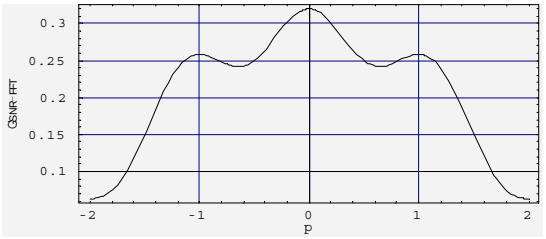

Figure 4-a. $G_{\text{SNR-FFT}}$ curve with $|q|$=2.1

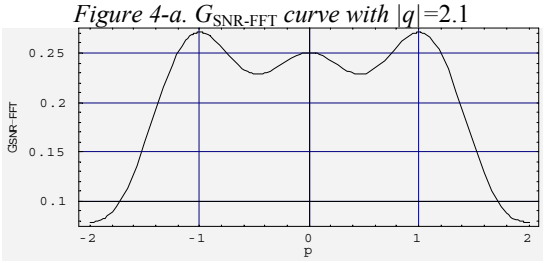

Figure 4-b. $G_{\text{SNR-FFT}}$ curve with $|q|$=2.2

According to the definition $q = \sqrt{\xi_0} \cdot T$ and $\xi_0 = 2a/\lambda$, the maximum integration time of FFT can be calculated by $T_{\max} = q_0\sqrt{\lambda/2a_{\min}}$. The ability of FFT to accumulate the energy of echo signal is limited by the maximum integration time, which restricts the detection performance.

3.2. Detection Performance of FrFT for Constant Acceleration Motion

Recently, FrFT attracts increasing attention in signal processing field. Almeida analysed the relation between FrFT and WVD, and interpreted it as a rotation operator in the time-frequency plane [11], which can be considered as a counter clockwise rotation from the time axis to the u axis with a rotation angle β. The FrFT of signal $x(t)$ is defined as

$$X_\beta(u) = F^\rho[x(t)] = \int_{-\infty}^{\infty} x(t)K_\beta(t,u)dt$$
$$K_\beta(t,u) = \begin{cases} A_\beta \cdot \exp\left(\mathrm{j}\pi\left(\cot\beta(t^2+u^2) - 2ut\csc\beta\right)\right) \\ \qquad \beta \ne n\pi \\ \delta(t-u), \beta = 2n\pi; \\ \delta(t+u), \beta = (2n+1)\pi \end{cases} \quad (14)$$

where ρ is called the order of FrFT and can be any real number, β=$\rho\pi/2$, F^ρ[.] denotes the FrFT operator, $K_\beta(t,u)$ is the kernel of FrFT and $A_\beta = \exp\left(-\mathrm{j}\pi\,\mathrm{sgn}(\sin\beta)/4 + \mathrm{j}\beta/2\right)\Big/\sqrt{|\sin\beta|}$. The decomposition expression [6] of discrete FrFT (DFrFT) is given by

$$X_\beta(m/\Delta l) = \left(A_\beta/\Delta l\right) \times \sum_{n=-N/2}^{N/2} \exp\left(\mathrm{j}\pi\left(\zeta m^2 - 2\eta mn + \zeta n^2\right)\Big/(\Delta l)^2\right) x\left(n/\Delta l\right) \quad (15)$$

where X_β(m) denotes the DFrFT of $x(t)$, ζ=-cotβ, η=-cscβ, N+1=FT and the normalized factor $\Delta l = \sqrt{N+1}$. Consider an echo signal $u(t) = r'(t) + e(t)$, where $e(t)$ is additive WGN. It is easily to obtain the following expression.

$$E\left[\left|U_\beta(m)\right|^2\right] = E\left[\left|R_\beta(m) + N_\beta(m)\right|^2\right] = \left|R_\beta(m)\right|^2/(N+1) + \sigma^2 A_\beta{}^2 \quad (16)$$

$U_\beta(m)$, $R_\beta(m)$ and $N_\beta(m)$ denote the DFrFT of $u(t)$, $r'(t)$ and $e(t)$ respectively. The variance of $e(t)$ is σ^2. We also have

$$Var\left[\left|U_\beta(m)\right|^2\right] = E\left[\left|U_\beta(m)\right|^4\right] - E\left[\left|U_\beta(m)\right|^2\right]^2 = 2\left|R_\beta(m)\right|^2 \cdot \sigma^2 A_\beta{}^2/(N+1) + \left(\sigma^2 A_\beta{}^2\right)^2 \quad (17)$$

According to the definition of output SNR proposed in [4], we define the output SNR of DFrFT as

$$SNR_{\text{out}} = \left|R_\beta(m)\right|^4 \Big/ Var\left[\left|U_\beta(m)\right|^2\right]\Big|_{\beta=\beta_0, m=m_0} \quad (18)$$

Using Eq. 18 and $\left|R_\beta(m)\right|^2\Big|_{\beta=\beta_0, m=m_0} = b^2 A_\beta{}^2 (N+1)$, we obtain

$$G_{\text{SNR-FrFT}} = SNR_{\text{MF}} / (2SNR_{\text{MF}} + 1) \tag{19}$$

The Eq. 19 indicates that $G_{\text{SNR-FrFT}}$ increases with SNR_{MF}. By the analysis above, there is no restriction for the integration time of FrFT. FrFT compensates the phase shift caused by the velocity and the acceleration, thus the echo energy is accumulated effectively and the detection performance is enhanced.

Fig. 5 illustrates the SNR gain of FrFT compared with FFT versus SNR_{MF} at different H with λ=0.25m, T=0.5s, $\theta_{\min}=\pi/6$ and $\theta_{\max}=\pi/2$, which are the typical value of L-band radar system. The maximum integration time of FFT is in direct proportion to the wavelength λ, so the SNR gain of FrFT compared with FFT will be higher when the emission signal frequency increases for detecting small size debris. Based on the FrFT filtering and inverse FrFT, the FrFT approach also can be applied in the situation of multi-targets [12].

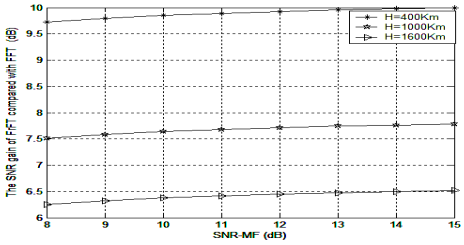

Figure 5. SNR gain of FrFT compared with FFT versus SNR_{MF} at different H

4. ACCURACY OF PARAMETER ESTIMATION BY FRFT

The performance of parameter estimation is usually evaluated by the statistical characteristics of the estimates. The accuracy of FrFT is evaluated by a first order perturbation analysis. The detection statistics can be expressed as

$$\left|U_\beta(m)\right|^2 = \left|R_\beta(m)\right|^2 + 2\,\text{Re}\left[R_\beta(m)N_\beta^*(m)\right] + \left|N_\beta(m)\right|^2 \tag{20}$$

Because the value of rotation angle β is arbitrary between 0 and π, the search for parameters (β_0,m_0) is equivalent to the search of (f_0,ξ_0) using the interpolation technique. Substituting the expressions $f=m\cdot\csc\beta$ and $\xi=m\cdot\cot\beta$ into Eq. 15, where f and ξ are normalized by sampling frequency F, we obtain

$$\begin{aligned}
&\left|U(f,\xi)\right|^2 = \left|R(f,\xi)\right|^2 + \left|N'(f,\xi)\right|^2 \\
&\left|R(f,\xi)\right|^2 = C_0 \sum_{n=-N/2}^{N/2} \sum_{k=-N/2}^{N/2} C_1(n,k)\times \\
&\exp[-\text{j}2\pi f(n-k)/\Delta l - \text{j}\pi\xi(n^2-k^2)/\Delta l^2]
\end{aligned} \tag{21}$$

$$\begin{aligned}
&\left|N(f,\xi)\right|^2 = C_0 \sum_{n=-N/2}^{N/2} \sum_{k=-N/2}^{N/2} C_2(n,k)\times \\
&\exp[-\text{j}2\pi f(n-k)/\Delta l - \text{j}\pi\xi(n^2-k^2)/\Delta l^2] \\
&+2C_0 \cdot \sum_{n=-N/2}^{N/2} \sum_{k=-N/2}^{N/2} \\
&\text{Re}\left[C_3(n,k)\exp[-\text{j}2\pi f(n-k)/\Delta l - \text{j}\pi\xi(n^2-k^2)/\Delta l^2]\right]
\end{aligned} \tag{22}$$

where $C_1(n,k)=r'(n)r'^*(k)$, $C_2(n,k)=e(n)e^*(k)$, $C_3(n,k)=r'(n)e^*(k)$, $C_0=|A_\beta/\Delta l|^2$ and $(^*)$ means conjugate. Obviously, $|R(f,\xi)|^2$ is at its maximum value $(N+1)|A_\beta b|^2$ when $f=f_0'=-f_0(\Delta l/F)$ and $\xi=\xi_0'=-\xi_0(\Delta l/F)^2$. However, the coordinates of the maximum value of $|U(f,\xi)|^2$ are shifted from (f_0',ξ_0') to $(f_0'+\delta f_0',\xi_0'+\delta\xi_0')$ due to the perturbation caused by the noise. By the property of the peak point, we have the following expressions:

$$\begin{aligned}
&\partial\left|U(f,\xi)\right|^2/\partial f\Big|_{f=f_0'+\delta f_0',\xi=\xi_0'+\delta\xi_0'} = 0 \\
&\partial\left|U(f,\xi)\right|^2/\partial \xi\Big|_{f=f_0'+\delta f_0',\xi=\xi_0'+\delta\xi_0'} = 0
\end{aligned} \tag{23}$$

From which, as a first order approximation, we obtain

$$\begin{aligned}
&\frac{\partial\left|U(f,\xi)\right|^2}{\partial f} + \frac{\partial^2\left|U(f,\xi)\right|^2}{\partial f^2}\cdot\delta f_0' + \frac{\partial\left|U(f,\xi)\right|^2}{\partial f\partial\xi}\cdot\delta\xi_0'\Big|_{\substack{f=f_0'\\ \xi=\xi_0'}} \approx 0 \\
&\frac{\partial\left|U(f,\xi)\right|^2}{\partial \xi} + \frac{\partial^2\left|U(f,\xi)\right|^2}{\partial \xi^2}\cdot\delta\xi_0' + \frac{\partial\left|U(f,\xi)\right|^2}{\partial f\partial\xi}\cdot\delta f_0'\Big|_{\substack{f=f_0'\\ \xi=\xi_0'}} \approx 0
\end{aligned} \tag{24}$$

At $f=f_0'$, $\xi=\xi_0'$, we have

$$\begin{aligned}
&\partial\left|R(f,\xi)\right|^2/\partial f\Big|_{f=f_0';\xi=\xi_0'} = \partial\left|R(f,\xi)\right|^2/\partial\xi\Big|_{f=f_0';\xi=\xi_0'} = 0 \\
&\partial\left|N'(f,\xi)\right|^2/\partial f\partial\xi\Big|_{f=f_0';\xi=\xi_0'} = \partial^2\left|N'(f,\xi)\right|^2/\partial\xi^2\Big|_{f=f_0';\xi=\xi_0'} \\
&= \partial^2\left|N'(f,\xi)\right|^2/\partial f^2\Big|_{f=f_0';\xi=\xi_0'} = 0
\end{aligned} \tag{25}$$

Therefore, by introducing the constants

$$\begin{aligned}
&x = \frac{\partial\left|N'(f,\xi)\right|^2}{\partial f}\Big|_{\substack{f=f_0'\\ \xi=\xi_0'}} \qquad y = \frac{\partial\left|N'(f,\xi)\right|^2}{\partial \xi}\Big|_{\substack{f=f_0'\\ \xi=\xi_0'}} \\
&X = \frac{\partial^2\left|R(f,\xi)\right|^2}{\partial f^2}\Big|_{\substack{f=f_0'\\ \xi=\xi_0'}} \quad Y = \frac{\partial^2\left|R(f,\xi)\right|^2}{\partial \xi^2}\Big|_{\substack{f=f_0'\\ \xi=\xi_0'}} \\
&Z = \frac{\partial^2\left|R(f,\xi)\right|^2}{\partial f\partial\xi}\Big|_{\substack{f=f_0'\\ \xi=\xi_0'}}
\end{aligned} \tag{26}$$

It can be easily extracted from Eq. 24 that

$$\begin{aligned}\delta f_0' &= (Zy - Yx)\big/\left(XY - Z^2\right)\\ \delta\xi_0' &= (Zx - Xy)\big/\left(XY - Z^2\right)\end{aligned} \tag{27}$$

The constants X, Y and Z can be expressed as

$$\begin{aligned}X &= -\left|A_\beta\right|^2 (b\cdot 2\pi)^2 \left(N^2+2N\right)\big/6 \quad Z = 0\\ Y &= -\left|A_\beta\right|^2 (b\cdot \pi)^2 \left(N^4+4N^3+N^2-6N\right)\big/90(N+1)\end{aligned} \tag{28}$$

From Eqs. 20-22 and Eq. 25, we obtain the statistical characteristics of x and y.

$$\begin{aligned}X &= -\frac{1}{6}\left|A_\beta\right|^2 (b\cdot 2\pi)^2 \left(N^2+2N\right) \qquad Z = 0\\ Y &= -\frac{1}{90(N+1)}\left|A_\beta\right|^2 (b\cdot \pi)^2 \left(N^4+4N^3+N^2-6N\right)\end{aligned} \tag{29}$$

From Eq. 27 and Eq. 29, we have $E[\delta f_0']=0$, $E[\delta\xi_0']=0$, which means the parameters estimation by DFrFT is unbiased, at least at a first order approximation. The variance of $\delta f_0'$ and $\delta\xi_0'$ can be expressed as

$$\begin{aligned}Var[\delta f_0'] &= \frac{3(SNR_{MF}+1)(N+1)}{2\pi^2 SNR_{MF}{}^2\left(N^2+2N\right)}\\ Var[\delta\xi_0'] &= \frac{90(SNR_{MF}+1)(N+1)^2}{\pi^2 SNR_{MF}{}^2\left(N^4+4N^3+N^2-6N\right)}\end{aligned} \tag{30}$$

Usually, the sample number $N>>1$, so we get

$$\begin{aligned}Var[\delta f_0'] &\approx \frac{3(SNR_{MF}+1)}{2\pi^2 SNR_{MF}{}^2 N}\\ Var[\delta\xi_0'] &\approx \frac{90(SNR_{MF}+1)}{\pi^2 SNR_{MF}{}^2 N^2}\end{aligned} \tag{31}$$

where $(f_0',\xi_0')$is normalized by F from the values of (f_0,ξ_0), and $f_0'=-f_0(\Delta l/F)$, $\xi_0'=-\xi_0(\Delta l/F)^2$. Combing the expressions and Eq. 31, we get the approximate variance of f_0 and ξ_0.

$$\begin{aligned}Var[\delta f_0] &\approx \frac{3(SNR_{MF}+1)}{2\pi^2 SNR_{MF}{}^2 T^2}\\ Var[\delta\xi_0] &\approx \frac{90(SNR_{MF}+1)}{\pi^2 SNR_{MF}{}^2 T^4}\end{aligned} \tag{32}$$

If $SNR_{MF}=(N+1)b^2/\sigma^2 >> 1$, Eq. 32 can be rewritten as

$$Var[\delta f_0] \approx \frac{3}{2\pi^2 SNR_{MF} T^2} \quad Var[\delta\xi_0] \approx \frac{90}{\pi^2 SNR_{MF} T^4} \tag{33}$$

which corresponds with the CRLB derived in [13]. The following table presents the accuracy of parameters estimation by FrFT and their CRLB, where λ=0.25m, T=0.5s and F=200KHz.

Table 1. Accuracy of parameters estimation and CRLB with different SNR_{MF}

SNR_{MF}	$Var[f_0]$	$CRLB[f_0]$	$Var[\xi_0]$	$CRLB[\xi_0]$
7dB	0.1455	0.1213	34.92	29.11
9dB	0.0862	0.0765	20.68	18.37
11dB	0.0521	0.0483	12.51	11.59
13dB	0.0320	0.0305	7.679	7.312
15dB	0.0198	0.01922	4.760	4.614

5. CONCLUSIONS

The fractional Fourier transform is a newly developed time-frequency analysis tool and becomes more and more attractive in signal processing, especially in non-stationary signal processing field. In radar system for space debris surveillance, the velocity of targets change when they cross the radar FOV, which makes the detection performance of FFT degraded even invalidated. This paper presented a method for detection and parameters estimation based on FrFT. The method searches in 2-D, that is the chirp rate dimension and Doppler shift frequency dimension, and gets the parameters estimation at the same time. The proposed method enhanced the detection performance due to higher integration gain by accumulating the reflected energy effectively. Additionally, the theoretical analysis about the accuracy of parameters estimation was also provided. The results indicate that the enhancement in detection performance is considerable and the accuracy of parameters estimation is close to the CRLB. Furthermore, the proposed method is simple in computation and easy in implementation because DFrFT can be calculated using FFT.

6. REFERENCES

[1] R. L. Easton & J. J. Fleming, "The navy space surveillance system," *Proceedings of IRE*, vol. 48, pp. 663-669, 1960.

[2] T. H. Michal, J. P. Eglizeaud & J. Bouchard, "GRAVES:The new french system for space surveillance," *Proceedings of the Fourth European Conference on Space Debris,* pp. 18-20, April 2005.

[3] A. M. Haimovich, C. D. Peckham & J. G. Teti. "SAR imagery of moving targets: Application of time-frequency distributions for estimating motion parameters," *SPIE Hybrid Image and Signal Processing IV*, SPIE vol. 2238, pp. 238-247, 1994.

[4] S. Barbarossa, "Analysis of multicomponent LFM signals by a combined Wigner-Hough

transform," *IEEE Trans. on Signal Processing*, vol. 46, no. 6, pp. 1511-1515, 1995.

[5] Tian Xiao-hua, Liao Gui-sheng & Wu Yun-tao, "Joint estimation of Doppler and multipath time delay of overlapping echoes for LFM pulse radar," *ACTA Electronica Sinica*, vol. 30, no. 6, pp. 857-860, 2002.(in Chinese)

[6] H. M. Ozaktas, O. Arikan, M. A. Kutay & Gözde Bozdağl, "Digital computation of the fractional Fourier transform," *IEEE Transaction on Signal Processing*, vol. 44, no. 9, pp. 2141-2150, 1996.

[7] Irfan Ali, Naofal Al-Dhahir & John E Hershey, "Doppler characterization for LEO satellites," *IEEE Trans. on Communications*, vol. 46, no. 3, pp. 309-313, 1998.

[8] S. H. Knowles, R. H. Smith & W. B. Waltman, "Experimental observations of naval space surveillance satellite Signals with an out-of-plane receiving station," *Naval Research Laboratory*, 1982.

[9] E. J. Kelly & R. P. Wishner, "Matched-Filter theory for high-velocity, accelerating targets," *IRE Trans. on military electronics*, vol. 9, no. 1, pp. 56-69, 1965.

[10] V. H. Jain, W. L. Collins & D. C. Davis, "High-accuracy analog measurements via interpolated FFT," *IEEE Trans. Instrum. Meas.*, vol. 28, no. 1, pp. 113-122, 1979.

[11] L. B. Almeida, "The fractional Fourier transform and time-frequency representations," *IEEE Trans. on Signal Processing*, vol. 42, no. 11, pp. 3084-3091, 1994.

[12] Qi Lin, Tao Ran, Zhou Si-yong & Wang Yue, "Detection and parameter estimation of multicomponent LFM signal based on the fractional Fourier transform," *Science in China Ser. F Information Sciences*, vol. 33, no. 8, pp. 749-759, 2003.

[13] Shimon Peleg & Boaz Porat, "The Cramer-Rao lower bound for signals with constant amplitude and polynomial phase," *IEEE Trans. on Signal Processing*, vol. 39, no. 3, pp. 749-752, 1991.